Prog. Oceanog. Vol. 14, pp. 353–385, 1985.
Printed in Great Britain.

0079-6611/85 $0.00 + .50

A Model of the Seasonal Circulation in the Arabian Sea Forced by Observed Winds

MARK E. LUTHER and JAMES J. O'BRIEN

Mesoscale Air–Sea Interaction Group, The Florida State University, Tallahassee, Florida 32306, U.S.A.

Abstract – Results of a numerical model of the wind driven seasonal circulation in the Arabian Sea are presented, with particular emphasis on the ocean's response to the monsoon winds. The model equations are the fully nonlinear reduced gravity transport equations in spherical coordinates. The model resolution is 1/8° in the east–west direction and 1/4° in the north–south direction. The model basin geometry corresponds as closely as possible to that of the north-west Indian Ocean from 40°E to 73°E and from 10°S to 25°N, and includes the gulfs of Aden and Oman, and the islands of Socotra and the Seychelles. The southern boundary and a portion of the eastern boundary, from the equator to 6°S, representing the opening between the Maldives and the Chagos Archipelago, are open boundaries. At other boundaries, the no-slip condition is applied. The wind stress data used to force the model comes from the NOAA National Climate Center's TD-9757 Global Marine Sums data, which consists of monthly mean winds compiled on 1° squares from over 60 years of ship observations. These data are interpolated in time using the mean and first five Fourier harmonics at each point, and then interpolated linearly to the model grid. The model equations are integrated in time using centered finite differences in time and space (a leap-frog scheme), with lateral friction treated by a Dufort–Frankel scheme.

After a one year spin up, the model settles into a regular periodic seasonal cycle, even though the solution to the model equations is locally highly nonlinear, with large nonlinear eddies developing in the same location at the same time of year from one year to the next. The development of the model Somali Current system with the onset of the (northern hemisphere) summer monsoon is consistent with the available observations in the region. The model reproduces many of the observed features in this region, such as the two-gyre circulation pattern, and the timing and movement of these features corresponds well with their real world counterparts. The model also shows an eastward jet forming in late June to early July at 13°N, just to the east of Socotra. This jet is fed by flow coming out of the great whirl. The break down of the two-gyre pattern occurs in mid to late August, when the southern gyre breaks up into several smaller eddies, the northern-most of which coalesces with the great whirl. Numerous small cyclonic eddies develop along the Arabian coast, from the Gulf of Oman into the Gulf of Aden, in early to mid August, and persist well into the winter monsoon. The model shows that it is possible to simulate very complicated flows, if one has sufficient wind data, using fairly simple models with a realistic basin geometry.

1. INTRODUCTION

THE NORTHWEST Indian Ocean, the Arabian Sea, is unique among the world's oceans in that the winds over the ocean basin reverse semiannually, blowing from the southwest during the northern summer, and from the northeast during the northern winter (the southwest and northeast monsoons). The periodic reversals in the winds drive corresponding reversals in the currents of the upper ocean. These seasonal reversals of the wind and surface circulation over such a vast area are remarkable when compared to the seasonal signals in the Atlantic or Pacific Oceans. The Somali Current has surface velocities and mass transports that exceed those of the Gulf Stream but that change direction every six months. There are numerous eddies in the Arabian and Somali basins that recur on a seasonal basis. The Indian Ocean is thus an ideal place in which to study the time-dependent nature of the response of the ocean to changing winds.

The currents in the Arabian Sea basins evolve rapidly into a very complex pattern of eddies with the onset of the southwest monsoon. Associated with these eddies are very strong horizontal temperature gradients and current shears. BRUCE (1973, 1979, 1983) and BROWN, BRUCE and EVANS (1980) have described the eddies associated with the Somali Current system in some detail. Recent attention has focused on the two gyre nature of the Somali Current onset. SWALLOW and FIEUX (1982) have reviewed the available historical data and found that the two gyre circulation pattern, with one clockwise gyre situated south of 5°N and another between 5°N and 10°N, is usually present in June. It is the northern gyre that was dubbed the 'great whirl' by FINDLAY (1866). More recent observations, especially those during the 1979 Indian Ocean Experiment, have revealed more details of the development of the two gyre system. SWALLOW, MOLINARI, BRUCE, BROWN and EVANS (1983) have described the reversal of the Somali Current with onset of the southwest monsoon during 1979 using temperature, salinity and current measurements. These observations are summarized in SCHOTT (1983).

Very little attention has been paid to the northeast monsoon, from December to January, primarily because it is so much weaker than the southwest monsoon and therefore less dramatic. BRUCE (1983) describes the long term monthly mean wind stress patterns obtained from ship observations, for both monsoons, and relates these to the observed ocean circulation patterns. These same wind data for the Indian Ocean are described in an atlas by HASTENRATH and LAMB (1979).

The numerous eddies in the northern Arabian Sea have been observed by CAGLE and WHRITNER (1981) using satellite infrared imagery (Fig. 1). They find that the eddies appear to be controlled both by the wind forcing and by topographic features associated with the coastline geometry. The eddies persist for long periods of time and appear to strengthen and weaken without significant advection.

We have developed a wind-driven numerical model to investigate the seasonal cycle of currents in the Arabian Sea. The nonlinear model includes a realistic basin geometry and is forced by observed mean monthly winds on a high resolution mesh in spherical coordinates. There are several earlier models of the Indian Ocean. COX (1970) developed a multi-layer model that was driven by idealized seasonal winds and temperature. The model was integrated for two centuries to arrive at a steady annual signal. The slow response time of the very deepest layers in the model necessitated the very long integration. HURLBURT and THOMPSON (1976) were the first to demonstrate the highly nonlinear nature of the eddies that form in the Somali Current during the onset of the southwest monsoon. COX (1976) found that local forcing by the wind dominates during the onset of the monsoon, but that remote forcing by equatorially trapped waves may alter the flow at later times. COX (1979) found that the movement of the eddies was strongly influenced by the basin geometry. LIN and HURLBURT (1981) showed that the spin-up of the Somali Current system could be effectively modeled using only the first baroclinic mode. They also demonstrated that the temporal and spatial distribution of the wind stress is crucial in determining the location and movement of the eddies in the Somali Current. ANDERSON and MOORE (1979) considered the Somali Current as a free inertial cross-equatorial jet, forced by the southern hemisphere trades and fed by the South Equatorial Current (SEC) and the East African Coastal Current (EACC).

All previous models have considered only the response of the Indian Ocean to very idealized wind forcing, considering primarily the response of the western boundary region to the sudden onset of the southwest monsoon. No models to date have looked at the eddies found in the northern Arabian Sea. The model we present here examines the response of the Arabian Sea to

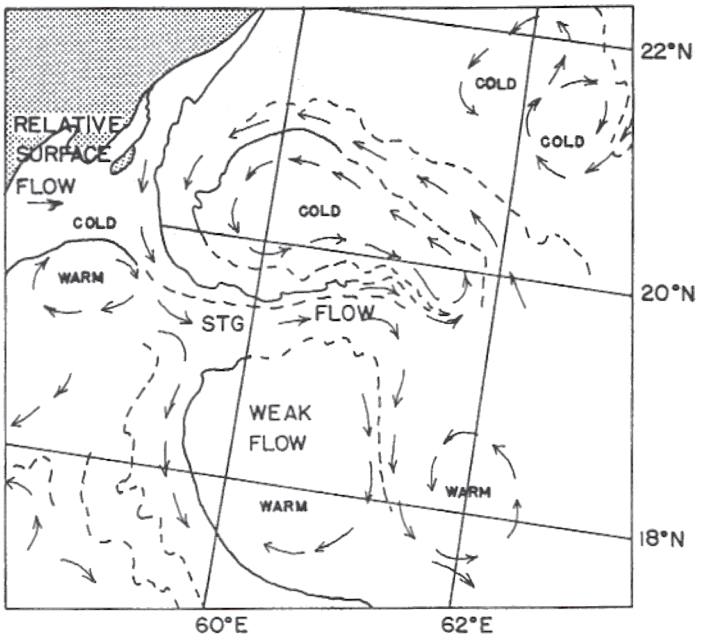

FIG. 1. Interpretation of infrared image of the coastal region south of the Gulf of Oman. Strong fronts are indicated by solid lines, weak fronts by dashed lines. A strong flow is indicated, associated with a major feature which propagates from the upwelling off the south tip of the Island of Masirah. A cold cyclonic eddy is indicated to the north of this tounge-like feature. A sequence of warm and cold eddies is indicated in progression down the coast of the Arabian Peninsula, and major features associated with points of land are repeated along the coast. Image was taken on 26 October 1980 by the NOAA-6 satellite. From CAGLE and WHRITNER (1981).

actual observed winds over the entire seasonal cycle. Other models of the onset of the Somali Current have considered only the spin-up of an ocean which is initially at rest in response to an impulsively applied, constant wind stress. As we will show, the past season's circulation influences the onset of both the (northern hemisphere) summer and winter Somali Current, so that to accurately model either, we must model the entire seasonal cycle.

We present here the results of one particular model simulation, and compare these results with recent observations. We focus our attention on the western boundary region, particularly the Somali Current regime, because that is where the most prominent variations occur and where the great majority of observations are made. This is not to say that currents in other areas of the Arabian Sea are not important, but the observations there are very limited. We prefer to concentrate here on a description of the model and to emphasize the agreement between the model results and observations. We will leave a detailed analysis of the model dynamics to future papers.

2. MODEL FORMULATION

To model the upper ocean response to an applied wind stress, we assume that the ocean consists of two incompressible, hydrostatic, homogeneous layers of slightly different densities, ρ_1 and ρ_2, with the interface between the two layers representing the pycnocline. We make the

further simplifying assumption that at some depth in the lower layer, the horizontal pressure gradient vanishes. This has the effect of eliminating the barotropic mode from the problem. The response of the system then consists of a single baroclinic mode. In fact, observations indicate that the first baroclinic mode dominates the Somali Current response to wind forcing (DÜING, 1978). The equations governing the motion in the upper layer for this mode are the so-called reduced gravity equations. Many investigators have used the linearlized form of these equations to model the tropical Atlantic and Pacific oceans (cf. ADAMEC and O'BRIEN, 1978; CANE, 1979a, b; KINDLE, 1979; BUSALACCHI and O'BRIEN, 1980), while others have used the fully nonlinear form to model the Somali Current (ANDERSON and MOORE, 1979; LIN and HURLBURT, 1981).

For this model, we use the fully nonlinear reduced gravity transport equations. Due to the latitudinal extent of the Arabian Sea, we use spherical coordinates, with ϕ (longitude) increasing eastward and θ (latitude) increasing northward. If we define the eastward and northward components of the upper layer transport as $U = uH$ and $V = vH$ respectively, where (u, v) are the depth-independent (ϕ, θ) velocity components in the upper layer and H is the thickness of the upper layer, the equations of motion are:

$$\frac{\partial U}{\partial t} + \frac{1}{a\cos\theta}\frac{\partial}{\partial\phi}\left(\frac{U^2}{H}\right) + \frac{1}{a}\frac{\partial}{\partial\theta}\left(\frac{UV}{H}\right) - (2\Omega\sin\theta)V = \frac{-g'}{2a\cos\theta}\frac{\partial H^2}{\partial\phi} + \frac{\tau^{(\phi)}}{\rho_1} + A\nabla^2 U \tag{2.1a}$$

$$\frac{\partial V}{\partial t} + \frac{1}{a\cos\theta}\frac{\partial}{\partial\phi}\left(\frac{UV}{H}\right) + \frac{1}{a}\frac{\partial}{\partial\theta}\left(\frac{V^2}{H}\right) + (2\Omega\sin\theta)U = \frac{-g'}{2a}\frac{\partial H^2}{\partial\theta} + \frac{\tau^{(\theta)}}{\rho_1} + A\nabla^2 V \tag{2.1b}$$

$$\frac{\partial H}{\partial t} + \frac{1}{a\cos\theta}\left\{\frac{\partial U}{\partial\phi} + \frac{\partial}{\partial\theta}(V\cos\theta)\right\} = 0, \tag{2.1c}$$

where $g' = (\rho_2 - \rho_1)/\rho_2\, g$ is the reduced gravity, a is the earth's radius, Ω is the earth's rotation rate, and A is a kinematic eddy viscosity. The wind stress, $\vec{\tau} = (\tau^{(\phi)}, \tau^{(\theta)})$, is applied as a body force over the upper layer (CHARNEY, 1955). The transport form of the reduced gravity equations has the advantage that the continuity equation (2.1c) is linear. It also has the advantage that the discretization of the advective terms in (2.1a and b) involves spatial averaging of the dependent variables, thus improving the numerical stability of the solution.

For the model geometry, we simulate the coastline of the Arabian Sea from 40°E to 73°E and from 10°S to 25°N. The model geometry is shown in Fig. 2. The boundary conditions along all solid (land) boundaries are the no slip conditions:

$$u = v = 0.$$

The southern boundary along 10°S and a portion of the eastern boundary, from 6°S to the equator, are open boundaries, the boundary condition there being a variation of the Sommerfeld radiation condition developed by HURLBURT (1974) and described in CAMERLENGO and O'BRIEN (1980). The eastern boundary from the equator to the Gulf of Khambat is closed, and the no slip boundary condition applies there. This simulates the Laccadive and Maldive islands which close off the eastern side of the Arabian Sea. The south-eastern corner of the model basin is closed off by the Chagos Archipelago, and again, the no slip boundary condition applies along the coast of this island.

Equations (2.1) are solved numerically on a 135 x 74 finite difference mesh. The solution mesh is staggered in space as shown in Fig. 3. The model resolution is 1/8° in the zonal direction ($\Delta\phi$) and 1/4° in the meridional direction ($\Delta\theta$). The equations of motion are integrated

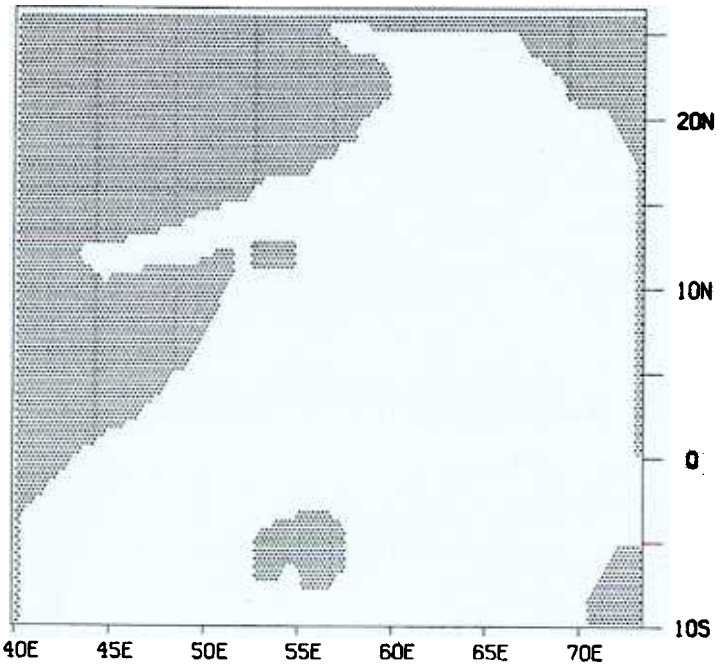

FIG. 2. Model geometry. Shadded areas indicate land boundaries. The shallow banks around Socotra, the Chagos, and the Seychelles are represented as land boundaries, as are the Maldives and Laccadives. The southern boundary and the eastern boundary, from 5°S to the equator, are open.

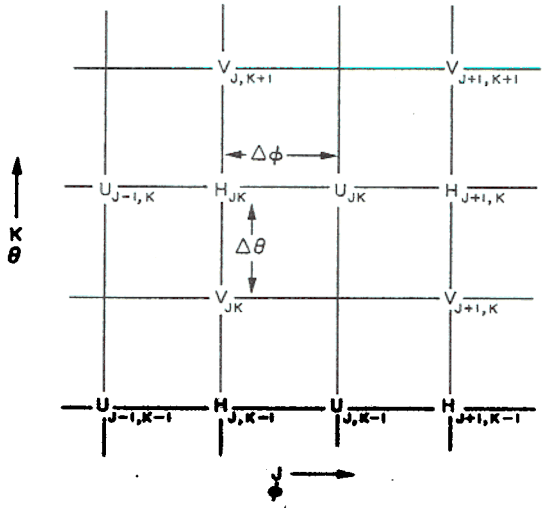

FIG. 3. Staggered mesh used in finite difference discretization of the governing equations, showing relative location of U, V and H points.

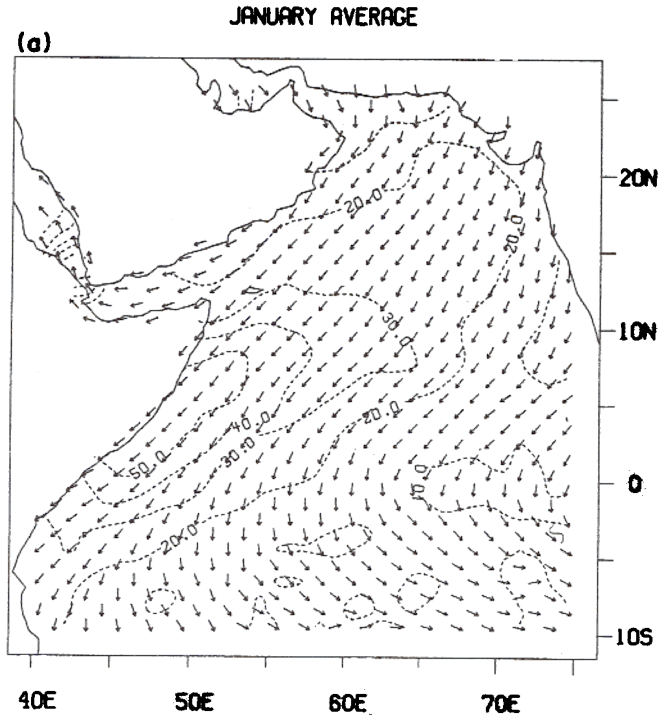
JANUARY AVERAGE
(a)
20N
10N
0
10S
40E
50E
60E
70E

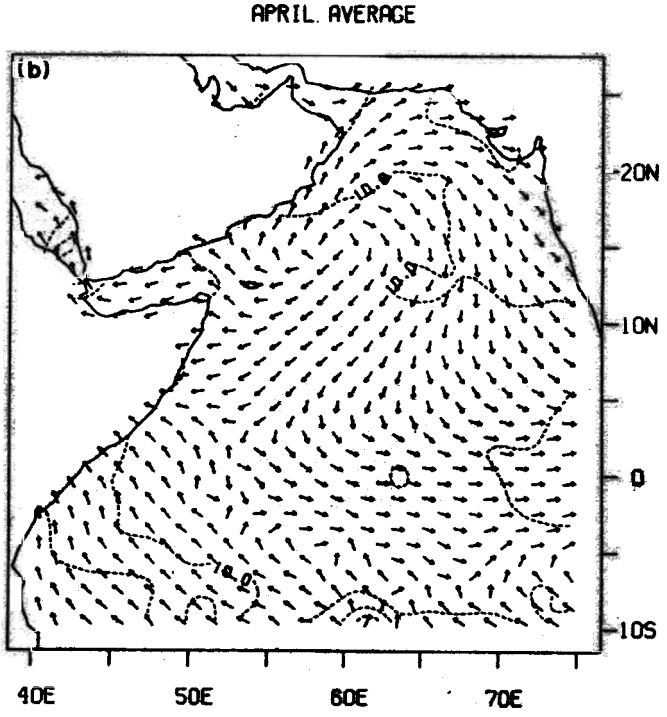
APRIL AVERAGE
(b)
20N
10N
0
10S
40E
50E
60E
70E

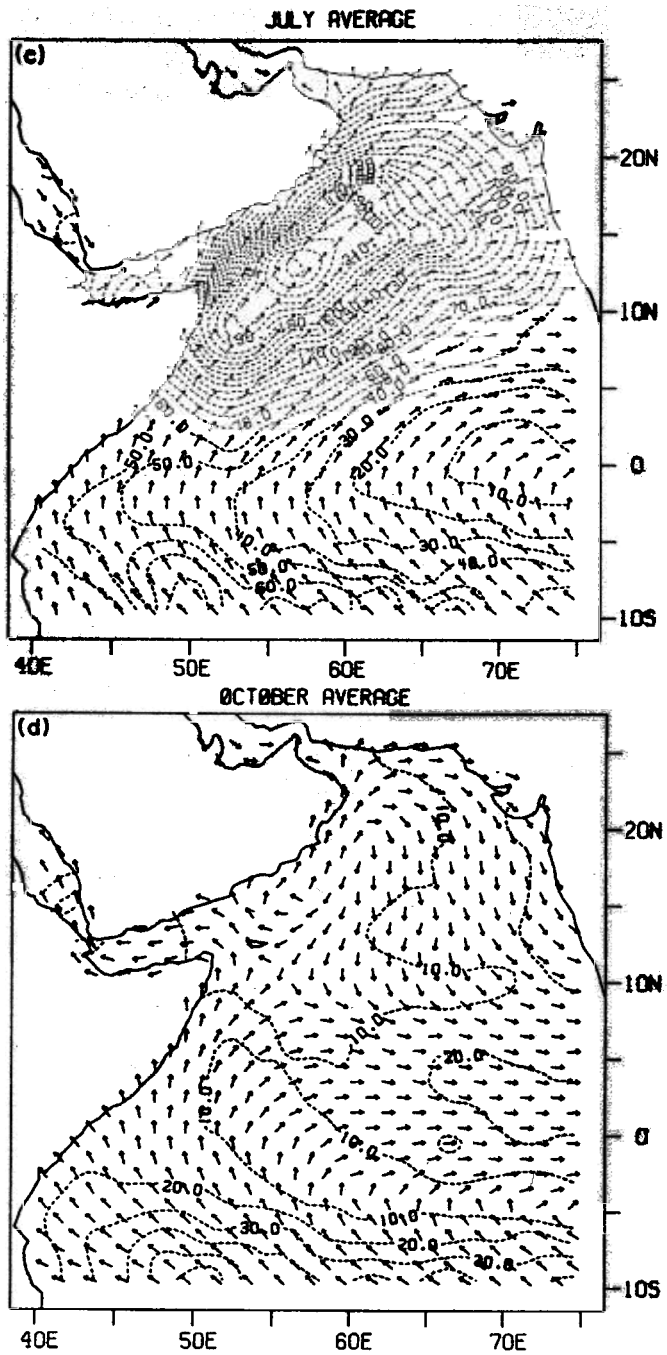

FIG. 4. Wind pseudo-stress vectors used as forcing for the model. Pseudo-stress is defined as $\hat{W}|\hat{W}|$, i.e., it is a measure of wind stress independent of drag coefficient. (a) January average, at the height of the northeast monsoon. (b) April average, at the transition from the northeast monsoon to the southwest monsoon. (c) July average, at the height of the southwest monsoon. (d) October average, at the transition from the southwest monsoon to the northeast monsoon. Contour interval is 10 m^2 s^{-2}.

in time using a leapfrog finite difference scheme, with a forward time difference used every 15th time step to eliminate the computational mode. The model time step is 30 min. The advective terms are computed by first averaging adjacent U, V and H values in space to form the desired product at the appropriate meshpoint and then forming the standard, second order accurate, centered finite difference approximation. The spatial averaging helps suppress nonlinear noise in the model. The viscous terms are treated with a Dufort–Frankel scheme.

In the linearized form of the reduced gravity equations, one must prescribe the linear phase speed for the particular baroclinic mode one wishes to model: $C^2 = g'H_0$. In the fully nonlinear form, there is no analogous phase speed parameter, only g'; however, in the numerical solution of (2.1) one must prescribe the initial upper layer thickness, H_0. This is analogous to prescribing an initial phase speed, but this does not remain constant as the model fields evolve, as the variations in H are large compared to H_0. The average thickness of the upper layer is not constant, due to inflow and outflow at the open boundaries during the seasonal cycle. The other free parameter in the model is the kinematic eddy viscosity, A. This cosmetic friction, sometimes referred to as sub-grid scale parameterization, is required to damp out the grid scale noise in the model to prevent this noise from growing through nonlinear interactions.

The model is forced using the climatological monthly mean winds. The wind data were obtained from the United States National Climate Center's Global Marine Sums TD-9757 data set, and consist of surface wind observations compiled on 1° squares from over 60 yr of ship reports. The monthly averages for some representative months are shown in Fig. 4. The data are interpolated in time using the mean and first five Fourier harmonics at each point in space, and then interpolated linearly in space to the model grid. The wind stress is computed from the bulk aerodynamic formula:

$$\vec{\tau} = \rho_a C_D \vec{W} |\vec{W}|, \tag{2.2}$$

where ρ_a is the density of air, C_D is a drag coefficient and $\vec{W}$ is the wind velocity. In the calculations to be presented here, we have taken $\rho_a = 1.2\,\mathrm{kg\,m^{-3}}$ and $C_D = 3.75 \times 10^{-3}$. Since the winds from which the stresses are computed are so highly averaged, we felt it unnecessary to use a variable drag coefficient, as the stress computed from the average wind is not the same as the average stress. The seemingly large value of the drag coefficient was chosen because the averaging process tends to underestimate the actual stress, and because reduced gravity models tend to underestimate the wind driven currents. The values of surface stress thus obtained agree well with those computed by HELLERMAN and ROSENSTEIN (1983). In an earlier version of this model, it was found that the circulation patterns produced were not sensitive to small variations in the magnitude of the drag coefficient. The model was also shown not to be sensitive to small variations in the parameters H_0 and A. Those parameter studies will be discussed in another paper. For the results presented here, we set $H_0 = 300\,\mathrm{m}$, $A = 750\,\mathrm{m^2\,s^{-1}}$ and the reduced gravity $g' = 0.03\,\mathrm{m\,s^{-2}}$.

3. RESULTS

The model is integrated from rest, beginning at 0000 GMT on 1 January, using an exponential taper with an e-folding time of 20 days to reduce the initial transients. For simplicity, the model year has 360 days, with each month having 30 days. The model fields spin up very quickly, due to the strong, time-varying nature of the forcing, and to the short response time of the equatorial ocean. After the first year, a seasonal cycle is established with a regular period, even though the solution is locally highly nonlinear. We present the results from the third year

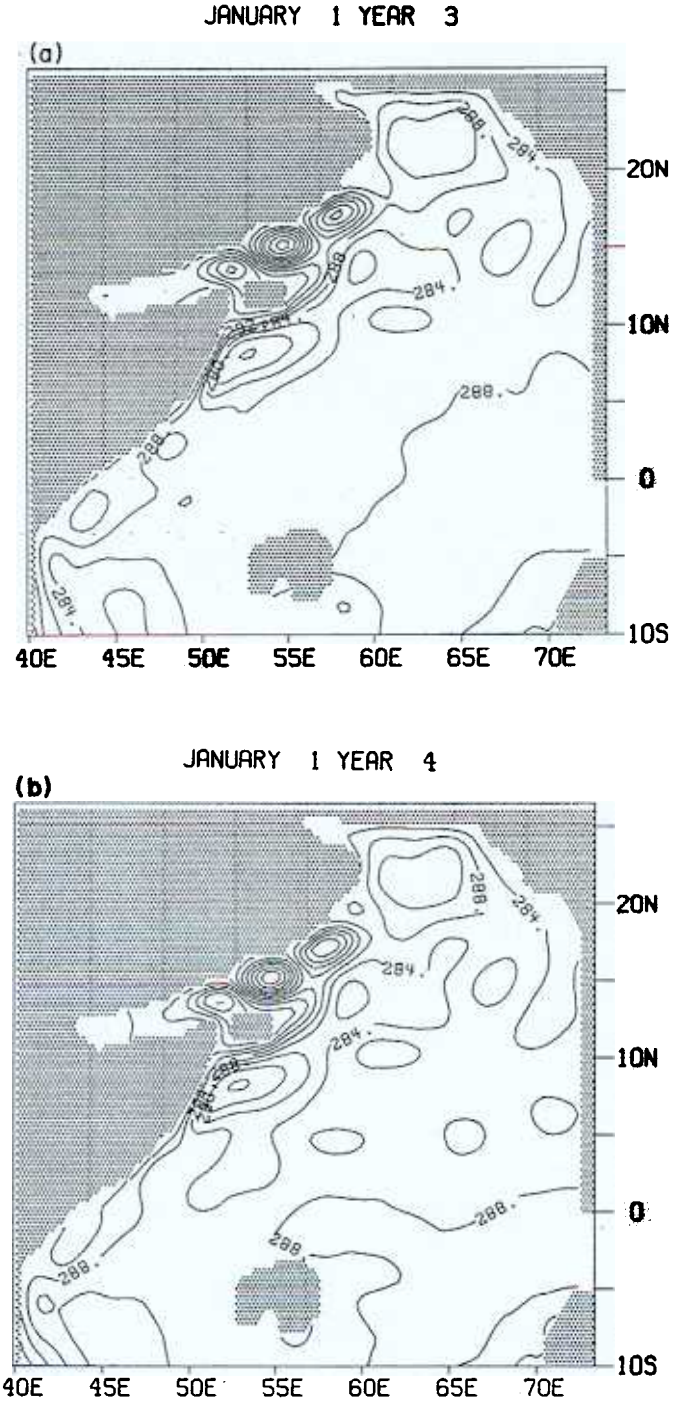

FIG. 5. (a) Instantaneous upper layer thickness for 0000 hr GMT on 1 January year 3. (b) Upper layer thickness for 1 January year 4. The seasonal cycle is established, and there is virtually no difference between the two years. Contour interval is 4 m.

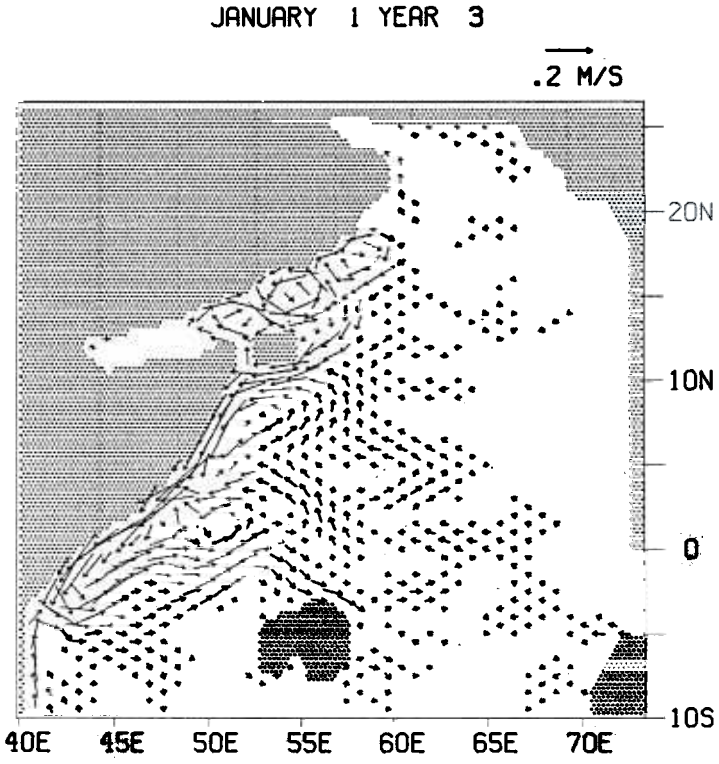

FIG. 6. Instantaneous upper layer velocity for 1 January year 3. Not all solution mesh points are shown. Vectors less than 0.02 m s^{-1} are surpressed, and vectors greater than 0.4 m s^{-1} are truncated. The winter Somali Current is fully developed. The eddies in the northern Arabian Sea off the Arabian Peninsula are remnants of the previous summer's circulation.

of integration. Figure 5 shows the H field at the end of the second and third years to illustrate the periodicity of the circulation. At this time the winter monsoon is at its peak intensity (see Fig. 4). The upper layer velocity for 1 January is shown in Fig. 6. The winter Somali Current is well developed, with southwestward flow along the western boundary from east of Socotra (12°N) all the way to 4°S, where it meets a northward coastal current, and both flow offshore. There is northward flow through the channel between Socotra and the Horn of Africa, and three large eddies north of Socotra, along the Arabian coast from the mouth of the Gulf of Aden to 20°N. In February, this circulation begins to break down into numerous weak eddies (Fig. 7), and by late March, we can see the beginnings of the summer Somali Current forming, with northward flow commencing between the equator and 4°S (Fig. 8), even though the local winds do not reverse for another two weeks. A weak anticyclonic feature develops just south of Socotra at this time, while the eddies north of Socotra have dissipated. There is an upwelling along the coast of the Arabian Peninsula from the Gulf of Oman to 15°N associated with a weak anticyclonic gyre.

By 1 April, northward flow exists all along the coast from 7°–8°S to 2°N, and by mid to late April, after the onset of northeastward winds, has become very strong (Fig. 9). This current turns offshore at 2°N, forming a broad gyre. A wedge-shaped area of shallower upper layer

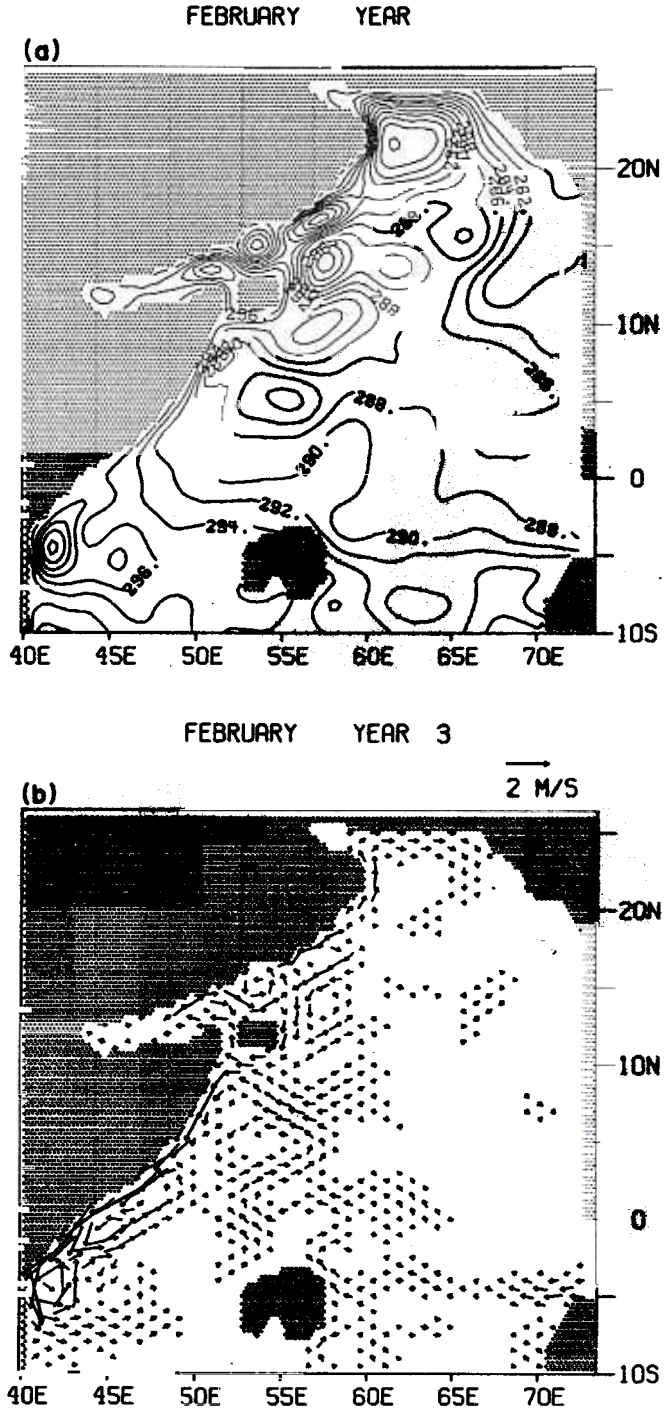

FIG. 7. (a) Same as Fig. 5 except for 1 February year 3. Contour interval is 2 m. (b) Same as Fig. 6.

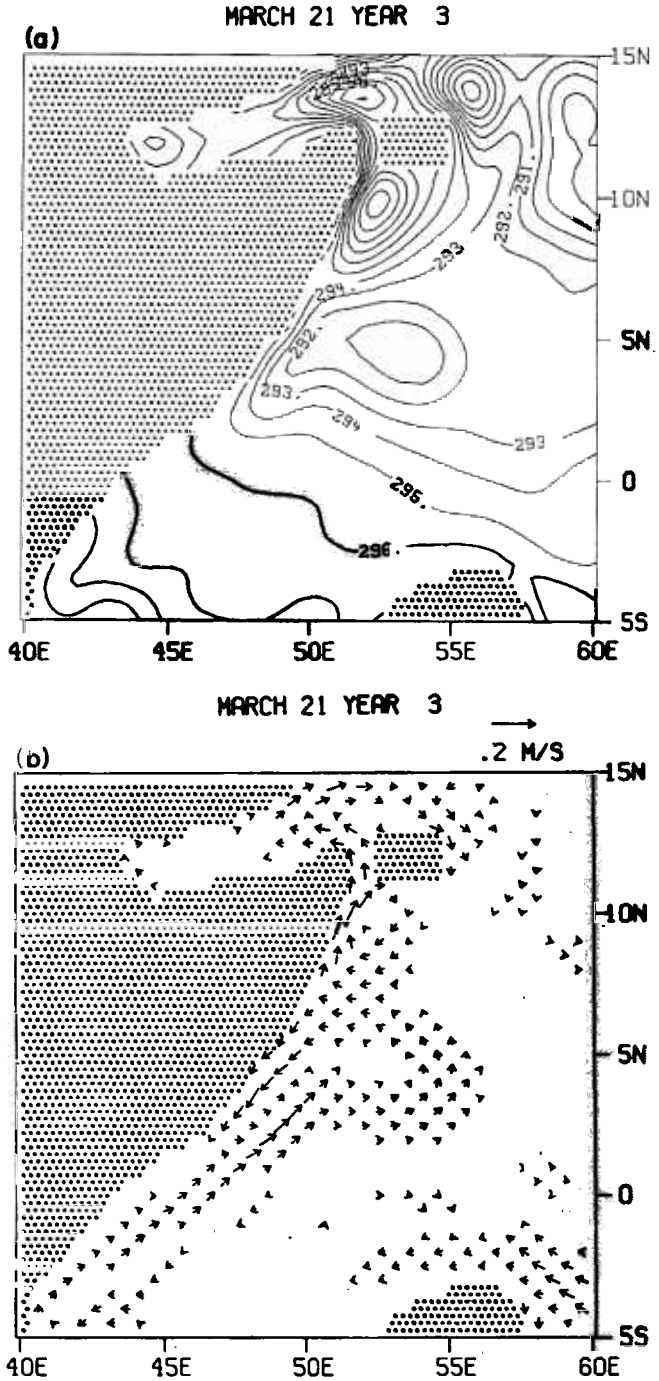

FIG. 8. (a) Instantaneous upper layer thickness for 0000 hr GMT on 21 March year 3 in the Somali Coast region. Contour interval is 1 m. (b) Instantaneous upper layer velocity. Again, vectors less than 0.02 m s^{-1} are surpressed and vectors greater than 0.4 m s^{-1} are truncated. Not all mesh points are shown.

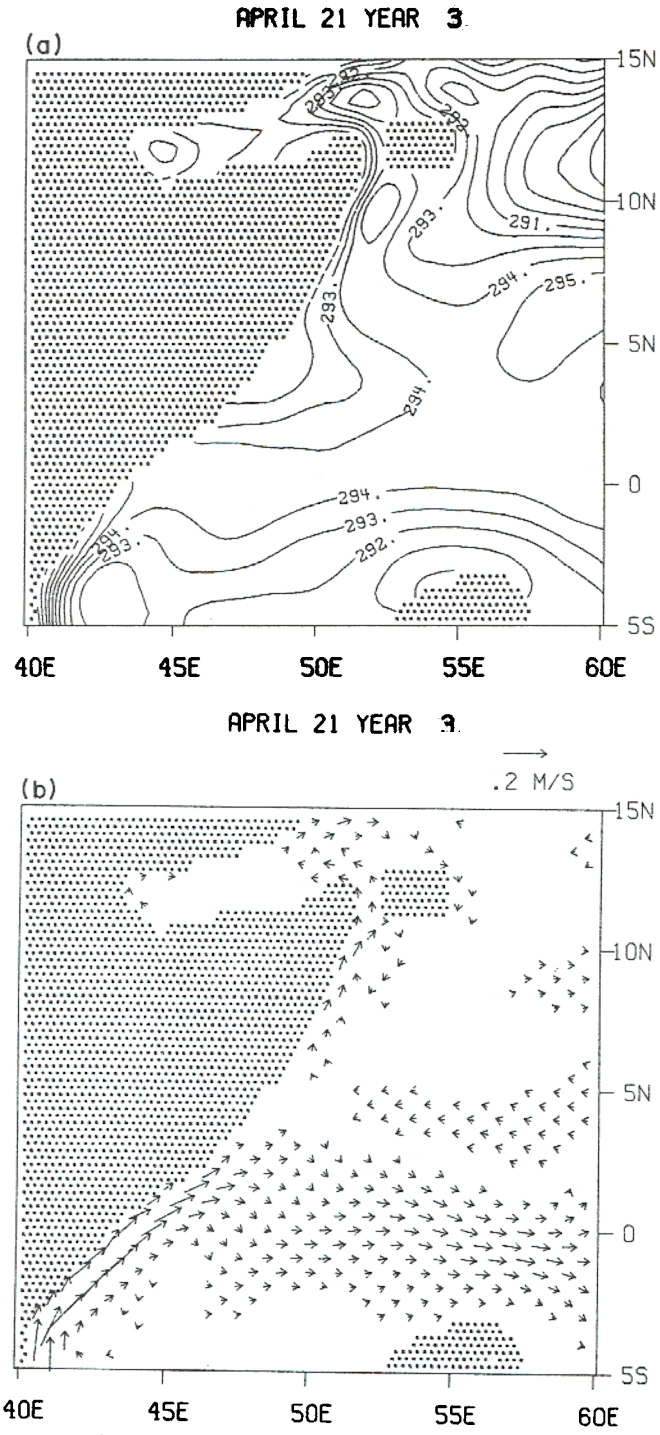

FIG. 9. (a) Same as Fig. 8(a) except for 21 April year 3. Contour interval 1 m. (b) Upper velocity, as in Fig. 8(b).

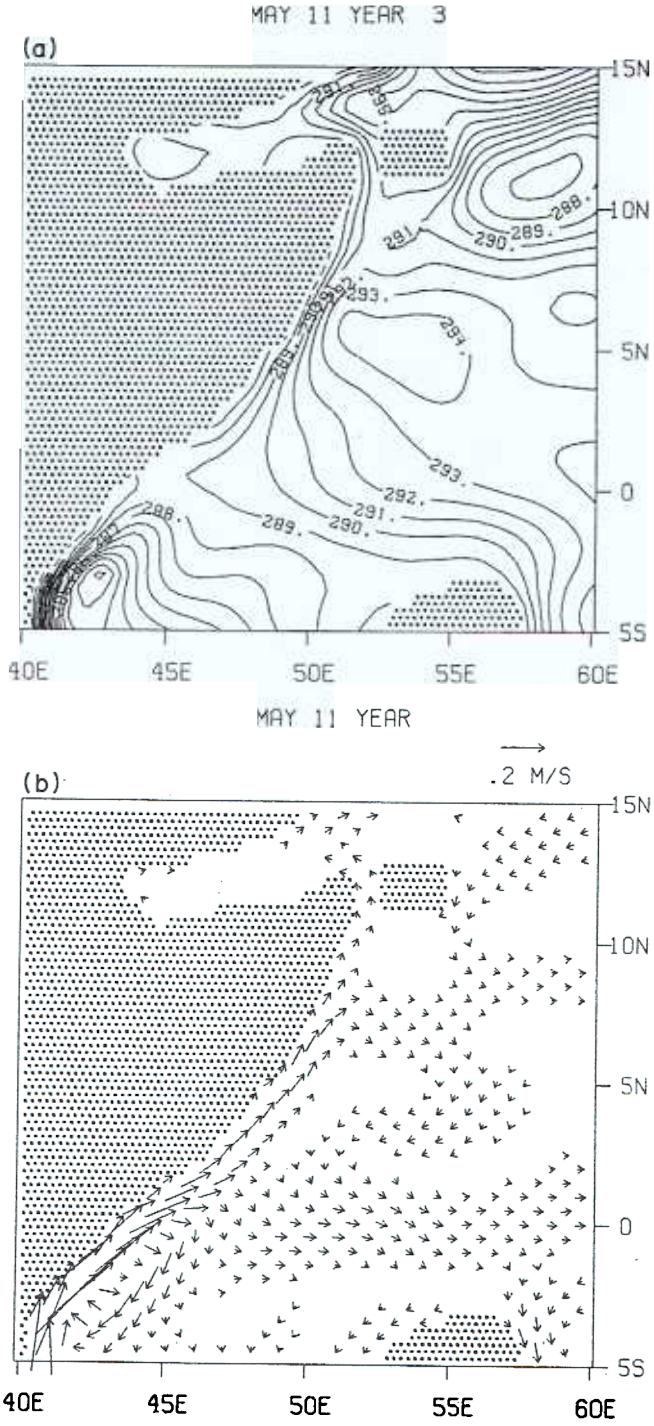

FIG. 10. (a) Same as Fig. 8(a) except for 11 May year 3. Contour interval is 1 m. (b) Upper layer velocity, as in Fig. 8(b).

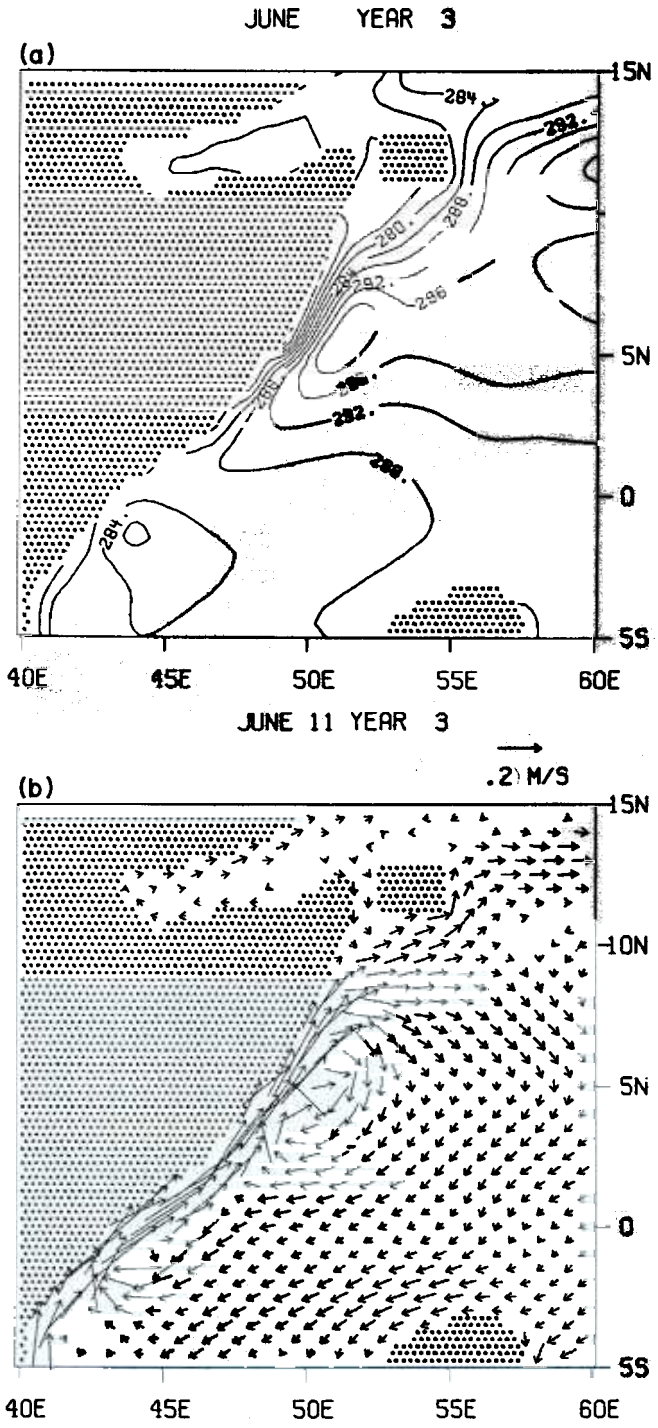

FIG. 11. (a) Same as Fig. 8(a) for 11 June year 3. Contour interval is 4 m. (b) Upper layer velocity, as in Fig. 8(b).

thickness, indicating upwelling, extends eastward from the Somali Coast from about 2°N to 4°N. North of this wedge, a weak anticyclonic circulation is beginning to form between 4°N and 11°N. This anticyclonic feature has become stronger by early to mid May, forming a second closed gyre (Fig. 10). The boundary current in the southern gyre still turns offshore at 2°N, and feeds an eastward equatorial current. There is also a strong recirculation region between 2°N and 3°S in the southern gyre. By late May, there is evidence of an upwelling wedge to the north of the northern gyre, at 9° to 10°N (Fig. 11). The two gyre Somali Current system now seems to be established, with the southern gyre located between 9°S and 2°N, and the northern gyre (the great whirl) located between 3°N and 9°N. At this time, however, the great whirl is still weak, and there is some flow from the southern gyre into the northern gyre. There is also strong upwelling along the Somali coast from 3°N to 9°N.

In early June, the situation is much the same, with the northern gyre increasing in intensity. By mid June, the offshore flow in the northern gyre splits just to the southeast of Socotra, with part of the current returning to the south in the interior of the gyre, and part flowing to the northeast, where it feeds an eastward jet at 13°N (Fig. 11). The separation region between the two gyres is characterized by several small eddies, from the equator to about 3°N. The locations of the gyres remain constant through mid July, although the currents continue to intensify. The boundary current separation region in the southern gyre, between the equator and 4°N, becomes increasingly unstable, with increasing eddy activity. In late July, after the wind stress begins to decrease, both gyres move northward. By 1 August (Fig. 12), the great whirl lies between 6°N and 11°N, and the southern gyre, which has now become two eddies rather than a single gyre, is located between 5°N and 8°–9°S. Flow through the channel between Socotra and the Horn of Africa increases at this time, and the mid-latitude jet at 13°N begins to meander considerably. A cyclonic eddy is beginning to form north of Socotra, in the mouth of the Gulf of Aden.

In late August, a large eddy separates from the southern gyre and moves northward, and by 1 September, is beginning to coalesce with the great whirl (Fig. 13). Another large eddy remains at the equator, between 2°N and 2°S, where it will stay until the onset of the winter monsoon. South of this eddy, there is still a northward flowing boundary current. The great whirl still lies between 6°N and 11°N, but flow through the channel and around the north side of Socotra has increased in intensity. The meandering jet has formed several eddies to the east and northeast of Socotra, and there are cyclonic eddies along the coast of the Arabian peninsula from the Gulf of Oman to the Gulf of Aden. During September, the great whirl weakens, and by 1 October, almost all the boundary current flow goes through the channel (Fig. 14), forming a closed anticyclonic gyre around the island of Socotra.

The winds off Somalia reverse in mid October and cause a strengthening of the currents in the southern part of the gyre around Socotra by 1 November (Fig. 15). This flow splits at 9.5°N, with part of it returning to the north through the channel, and the rest of it flowing southward along the coast to form the winter Somali Current. This current flows all the way to the equator, where it meets the northward flowing remnants of the summer Somali Current southern gyre. Both currents turn offshore into a meandering equatorial current. This offshore flow continues to push southward, moving to 3°S by 1 December (Fig. 16). Remnants of the summer anticyclonic flow persist to the north and east of Socotra throughout the winter monsoon. This pattern remains unchanged through December, and the following January the cycle repeats (Fig. 5).

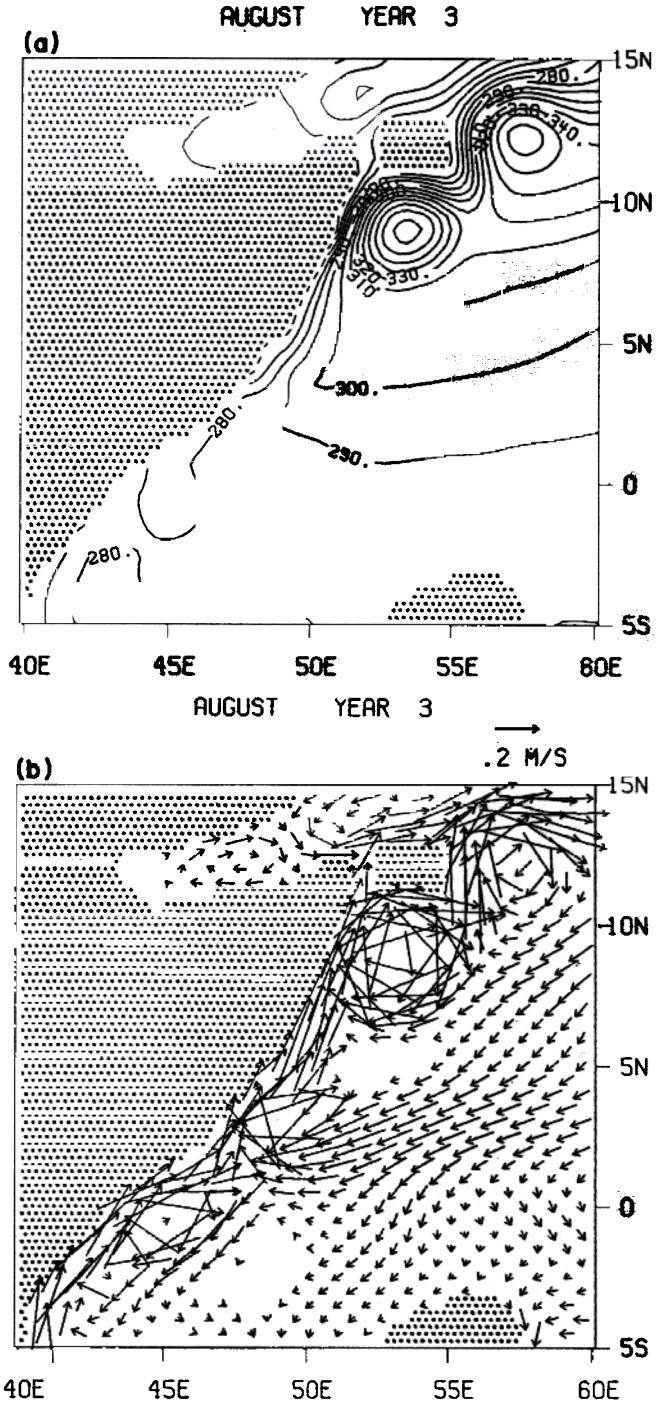

FIG. 12. (a) Same as Fig. 8(a) for 1 August year 3. Contour interval is 10 m. (b) Upper layer velocity, as in Fig. 8(b). At this time the great whirl is fully developed, and another eddy to the east of Socotra is clearly evident.

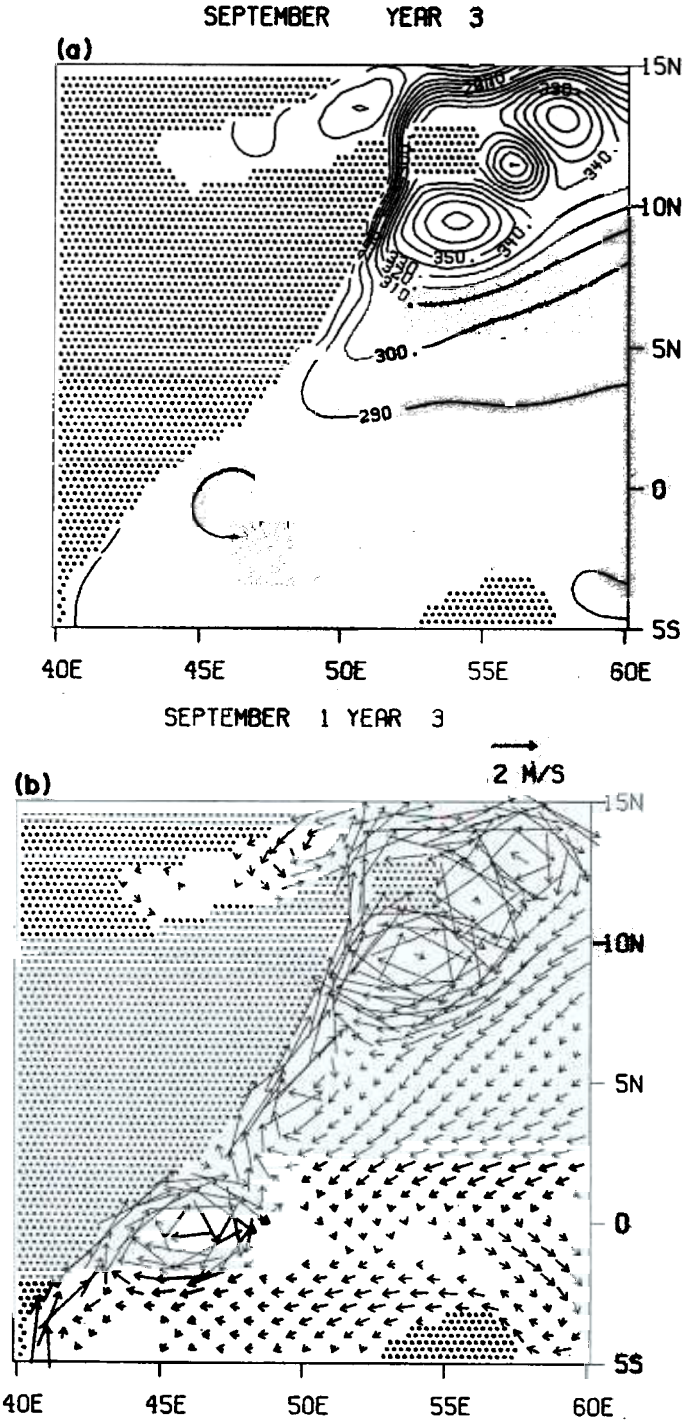

FIG. 13. (a) Same as Fig. 8(a) for 1 Ssptember year 3. Contour interval is 10 m. (b) Upper layer velocity, as in Fig. 8(b).

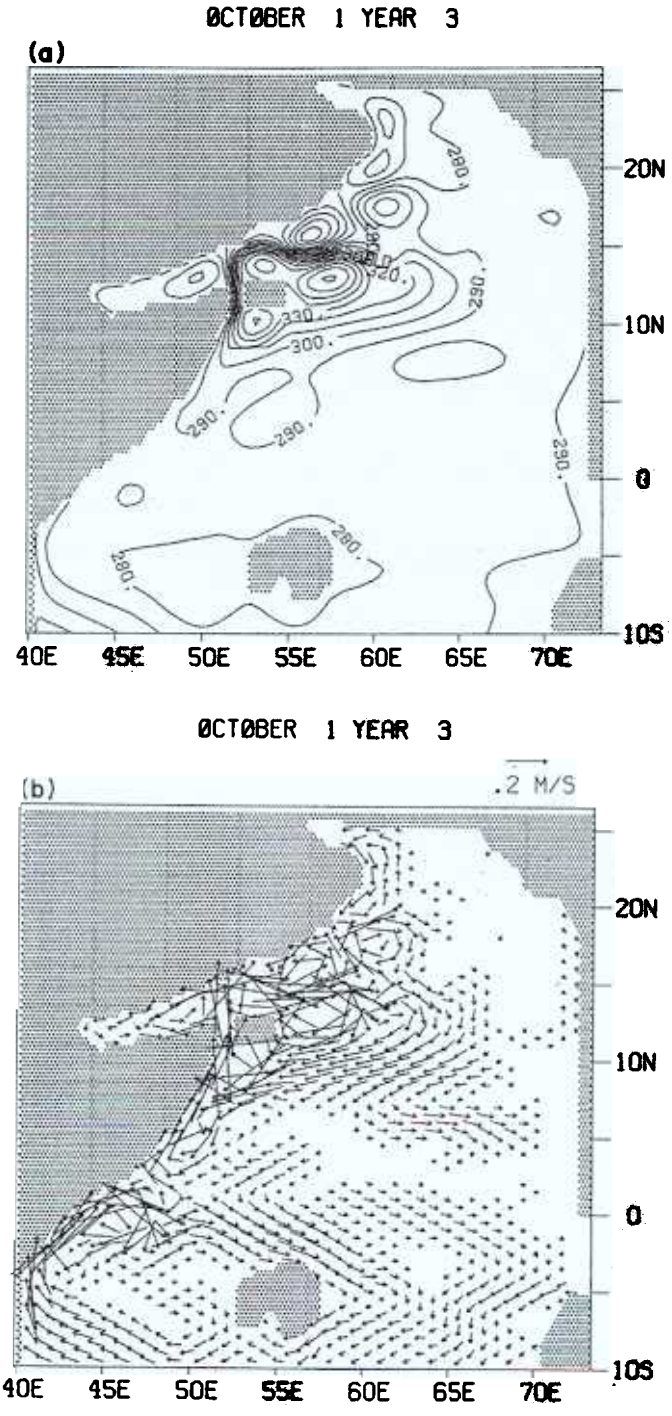

FIG. 14. (a) Same as Fig. 5 for 1 October year 3. Contour interval is 10 m. (b) Upper layer velocity, as in Fig. 6.

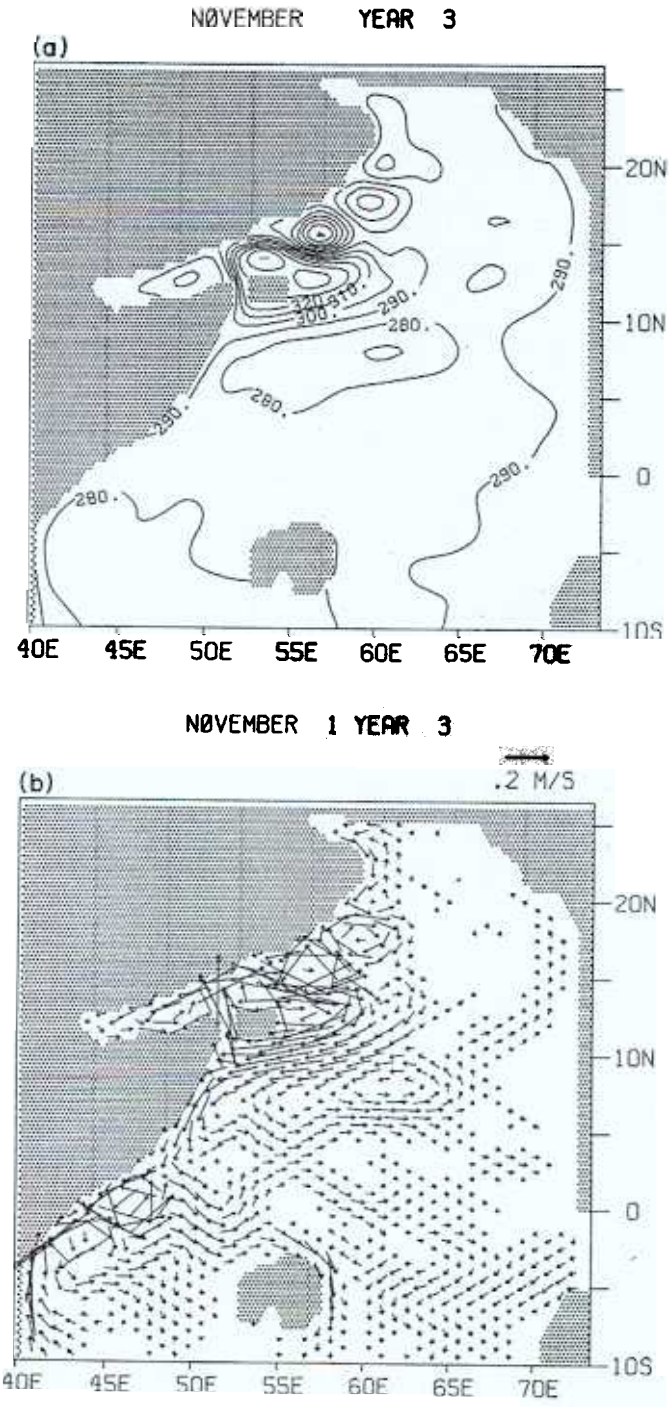

FIG. 15. (a) Same as Fig. 5 for 1 November year 3. Contour interval is 10 m. (b) Upper layer velocity, as in Fig. 6.

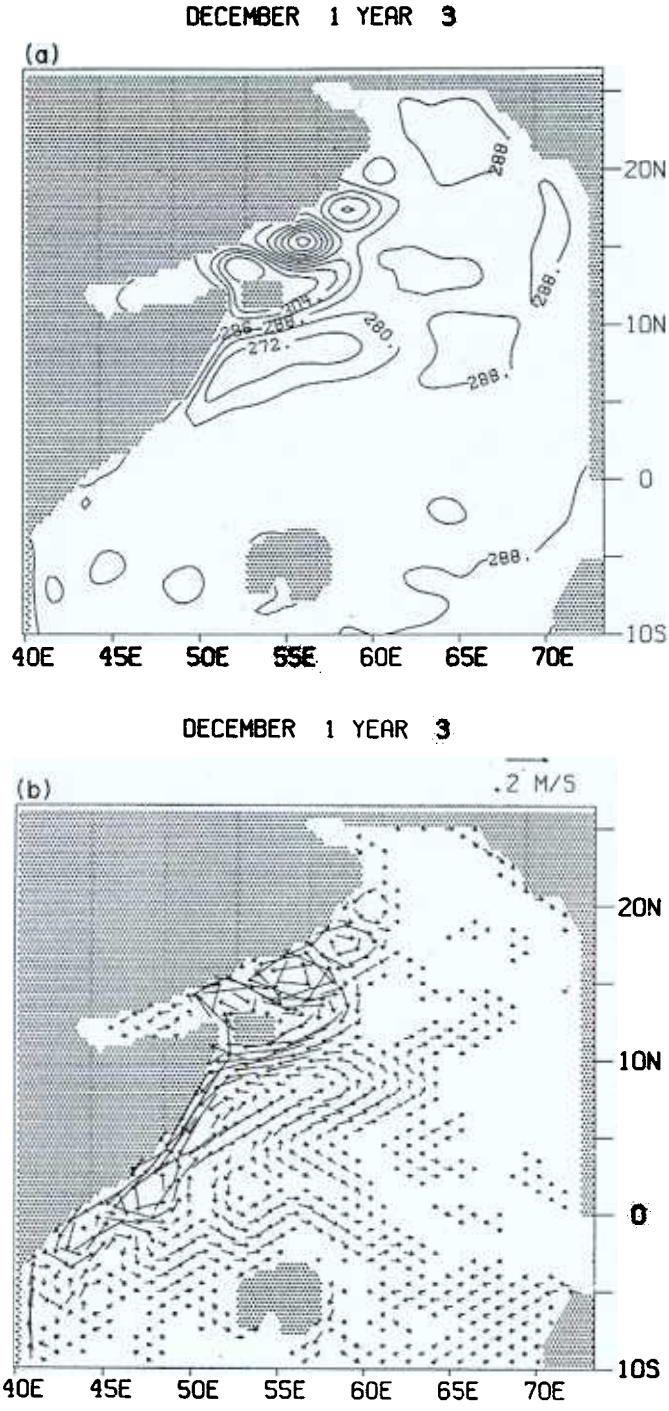

FIG. 16. (a) Same as Fig. 5 for 1 December year 3. Contour interval is 8 m. (b) Upper layer velocity, as in Fig. 6.

4. COMPARISON WITH OBSERVATIONS

Observations of currents and temperature in the Somali Current regime were, until recently, sparse at best, especially during the winter monsoon. SCHOTT (1983) provides a comprehensive summary of the recent observations in the area, concentrating mainly on the measurements during the Indian Ocean Experiment (INDEX) of 1979. SCHOTT (1983) summarizes the seasonal cycle of the Somali Current as follows:

> "1. During the winter monsoon, from November to February, the Somali Current flows southward along the coast from Ras Hafun to about 2°–3°S where it meets the East African Coast Current and then both turn offshore into the Equatorial Counter Current."

In Figs 6, 7, 15 and 16 we see the development of the winter Somali Current and the East African Coastal Current in the model. The Equatorial Counter Current in the model forms near the equator in early November and moves southward, reaching 4°S by 1 January; however, in the model, southward flow extends to 7°S by 1 February.

> "2. In early March, when winds off Northern Somali are still southward, the current north of 5°N already reverses northward. This is due to the wind stress curl distribution off Somalia which has a maximum at about 5°N causing strong onshore flow at that latitude. Consequently, the surface flow at the Somali coast splits up into a northward and a southward branch at 5°N."

Figure 17 shows this occurring in the model at a slightly higher latitude, near 6.5°N. It is likely that the position of the maximum in the wind stress curl to which Schott refers varies from

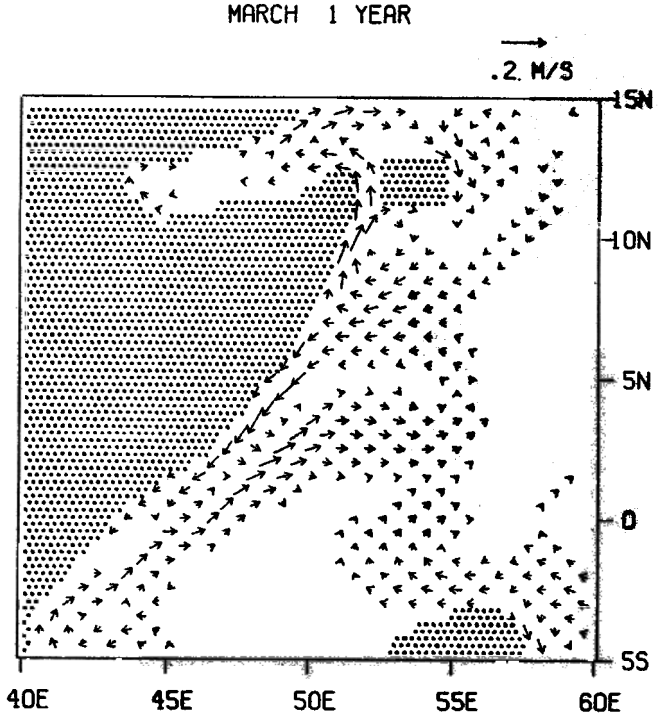

FIG. 17. Upper layer velocity for 11 March year 3, at the end of the northeast monsoon, as in Fig. 8.

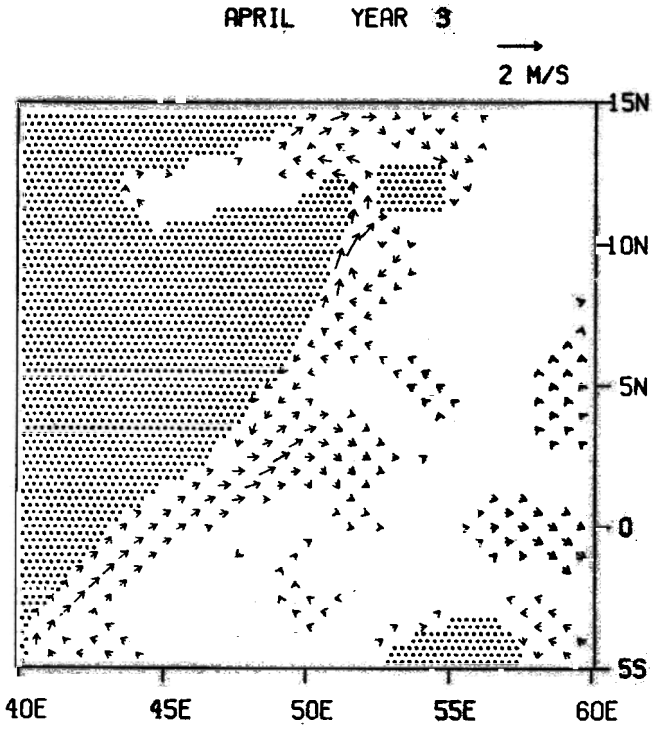

FIG. 18. Upper layer velocity for 1 April year 3, as in Fig. 8(b). Northward flow has commenced south of the equator.

year to year and was slightly farther south in 1979 than on average; however, 1.5° is not a very large difference.

> "3. In April, shortly after the occurrence of onshore and northward winds south of the equator, a shallow northward cross equatorial current develops which turns offshore north of the equator."

In Fig. 18, we see the model currents flowing northward across the equator and turning offshore between 1° and 2°N on 1 April.

> "The latitude of offshore turning migrates northward during April to May. A cold wedge of upwelled water develops along the coast north of the offshore turning flow. North of 5°N the surface flow continues to flow northward during this time . . ."

In Fig. 9, we see that the offshore turning flow is at about 3°N on 21 April, and that a large wedge-like feature is forming between 3°N and 5°N from a lifting of the pycnocline, indicating upwelling. To the north of this feature the flow is still northward.

> "4. In early May, the winds turn to southerly, parallel to the coast over the whole Somali Current regime. Coastal temperatures north of the equator drop simultaneously. The latitude of offshore turning flow is now 3°–4°N with strong coastal upwelling north of it. North of that offshore turn a typical upwelling regime develops with northward surface flow, an undercurrent and cold water along the coast."

The upper layer thickness in Fig. 10 shows a thinning of the upper layer, indicating cooler surface temperatures, from 1°N to 9°N along the Somali Coast. The offshore turning in the model Somali Current has moved back to the south, however, and is now at about 2°N. Again,

this could vary from year to year. To the north of 2°N, a typical upwelling regime does indeed exist, with northward surface flow and upward vertical velocities (as inferred from pycnocline movements) along the Somali Coast. Of course, there is no undercurrent in this model, since there is only one dynamically active layer.

> "5. When the final monsoon onset occurs, defined by strong winds off northern Somalia and a strong anticyclonic wind stress curl offshore, the northern gyre is generated within two weeks, most likely through Rossby waves excited by the offshore wind stress curl. Immediately upon the occurrence of strong coast-parallel winds, the coastal temperatures drop drastically and simultaneously north of 5°N. When the northern gyre is fully generated, coastal temperatures rise again. There is now a two gyre system in existence with offshore flow at 3°–4°N, an upwelling wedge north of it, and offshore flow again north of 9°N with a second upwelling wedge off Ras Hafun. This pattern stays about stationary until mid August."

Figure 11 shows the northern gyre well defined by 11 June with very strong upwelling along the coast. The strong winds off northern Somalia occur at about this time. The latitude of the offshore turning in the southern gyre is still about 2°N. It is suspected that Rossby waves excited by the wind stress curl play a part in generation of this northern gyre, but this has not yet been investigated fully. By mid July, this pattern has shifted northward slightly (Plate 1), and the locations of the offshore flows agree well with Schott's description. The upwelling wedges can be inferred from the vertical velocity as computed from the continuity equation. The warming of the coastal temperatures is not seen in the model, since no thermodynamics are included. The eastward jet in the model to the northeast of Socotra is essentially just an extension of the northern gyre. This pattern remains stationary until early to mid August.

> "6. The winds off northern Somalia start to decrease in September. In August or September, the two gyre system collapses rather suddenly. This is documented by the propagation of the southern cold wedge to the north. The northern cold wedge also moves northward and then back southward, and finally both seem to merge. A continuous boundary flow is then established . . ."

In Fig. 19, we see the beginning of the collapse of the two gyre system in the model. The northern portion of the southern gyre, which has become very unstable, separates and moves northward, eventually merging with the northern gyre to form a continuous boundary flow from 2°N to 10°N. In the model there is increasing flow through the channel west of Socotra. This flow may be unrealistic, in that the model channel is much wider than the passage between Abd al Kuri and Ras Aser. It would be helpful to know just how much flow actually does go through that passage. The model does not show the southern gyre merging completely with the northern gyre. A part of the southern gyre remains between 4°S and 1°N, with offshore flow at 1°N, and stays in this location until the onset of the winter monsoon.

> "7. After the coalescence of the two gyres the boundary current is stationary again, now as the conventionally known Somali Current, as it is displayed in textbooks and atlases, fed in the south by the East African Coast Current and the South Equatorial Current and flowing along the coast from 4°S to 10°N."

Here, the model results differ from the observations. The circulation pattern along the coast from 10°S to 10°N remains essentially unchanged from that in Figs 14 and 13 until the onset of the winter monsoon.

> "The onset of the northeast monsoon occurs in November: within a few days the currents along the coast turn southward."

In Fig. 15, we see that the model coastal currents reverse at about the same time as the winds due to the strengthening of the onshore flow in the southern part of the summer northern

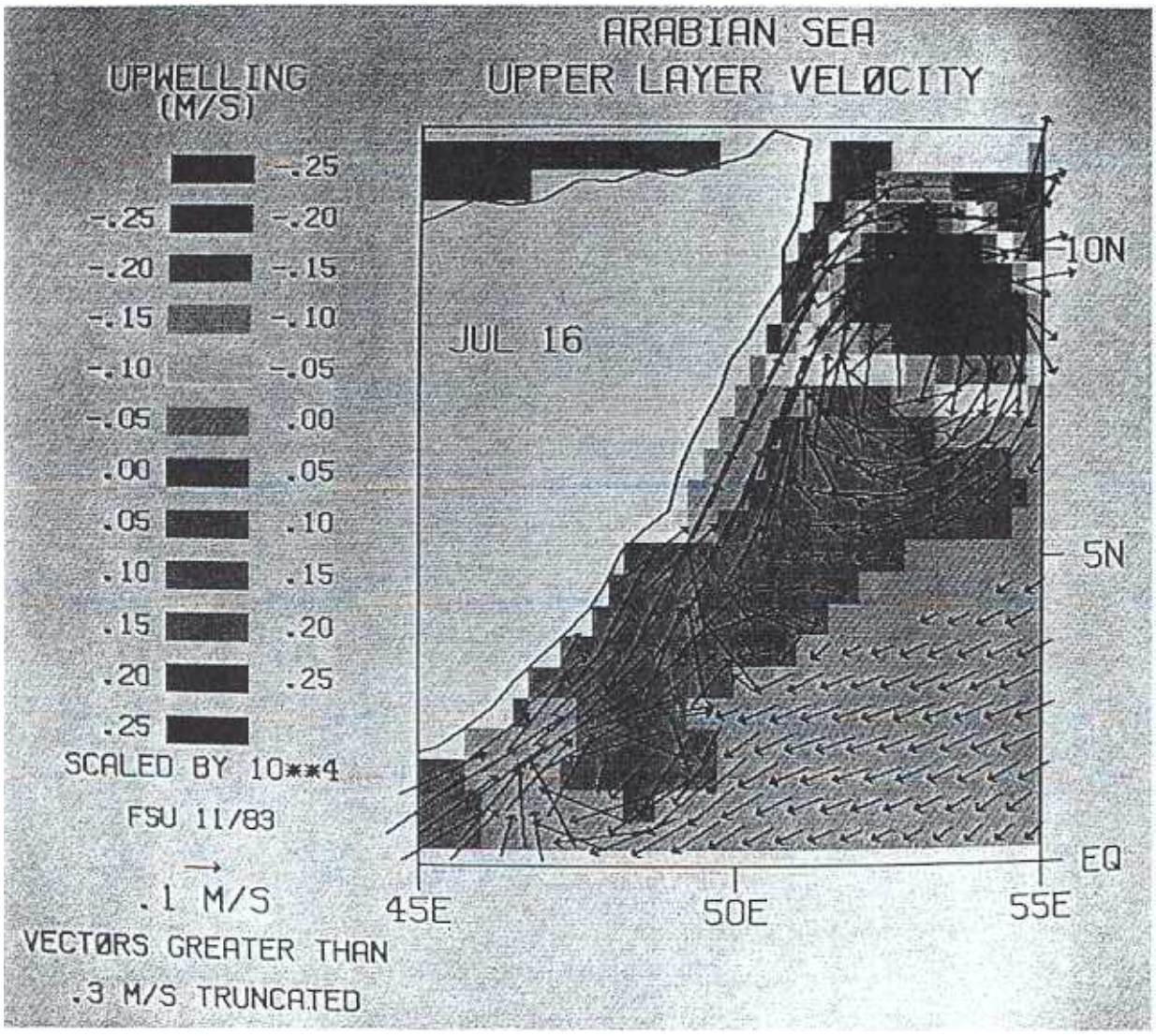

PLATE 1. Upper layer velocity for 16 July year 3. The great whirl and the upwelling wedges (blue areas) are clearly evident. Color scale represents vertical velocity at the interface as computed from the continuity equation. The velocity components have been averaged over 15 days centered on the 16th.

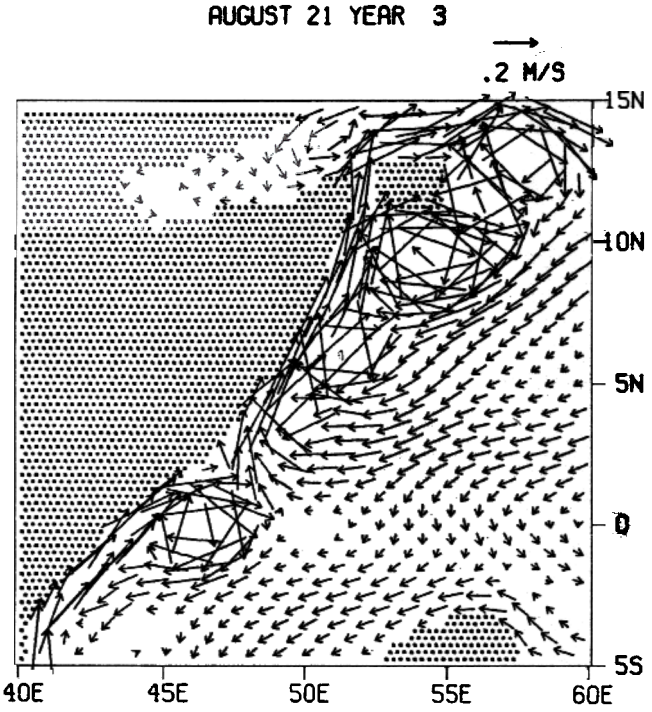

FIG. 19. Upper layer velocity for 21 August year 3, as in Fig. 8(b). The summer monsoon circulation is beginning to break up.

gyre. Thus, the onset of the winter monsoon is influenced strongly by the previous summer's circulation.

BRUCE (1983) examined the wind stress field over the western Indian Ocean derived from the same data base as our wind stress. He compared the wind stress and wind stress curl patterns with the observed circulation and thermocline topography. Even though he used a much more complicated analysis scheme, his wind stress patterns look much the same as ours. Figure 20 shows our average wind stress curl for May, June and July (in BRUCE, 1983, Figs 3, 4 and 5). If we compare these with the upper layer thickness for 1 June, July and August (Fig. 21) we see a very similar relationship to that described by BRUCE (1983). The maxima in upper layer thickness correspond to the regions of negative wind stress curl during the previous month, as one would expect, especially in July and August. The anticyclonic gyre to the south of Socotra (the great whirl) on 1 July is centered at the same latitude and to the west of the minimum in wind stress curl for June. Similarly, the broad gyre to the east of Socotra corresponds to the large region of minimum wind stress curl at that same location in June, while the core of the Somali Current follows the line of zero curl. By 1 August, the great whirl has moved northward, as has the minimum curl. The gyre to the east of Socotra has tightened into what BRUCE (1979) called the Socotra eddy, and the thermocline topography (upper layer thickness) is still closely related to the wind stress curl. The westward displacement of the maxima in upper layer thickness relative to the minima in wind stress curl is indicative of westward propagating Rossby waves radiating from the curl minima.

SWALLOW, MOLINAR, BRUCE, BROWN and EVANS (1983) present charts of surface currents and depth of the 20°C isotherm during the southwest monsoon of 1979. There is

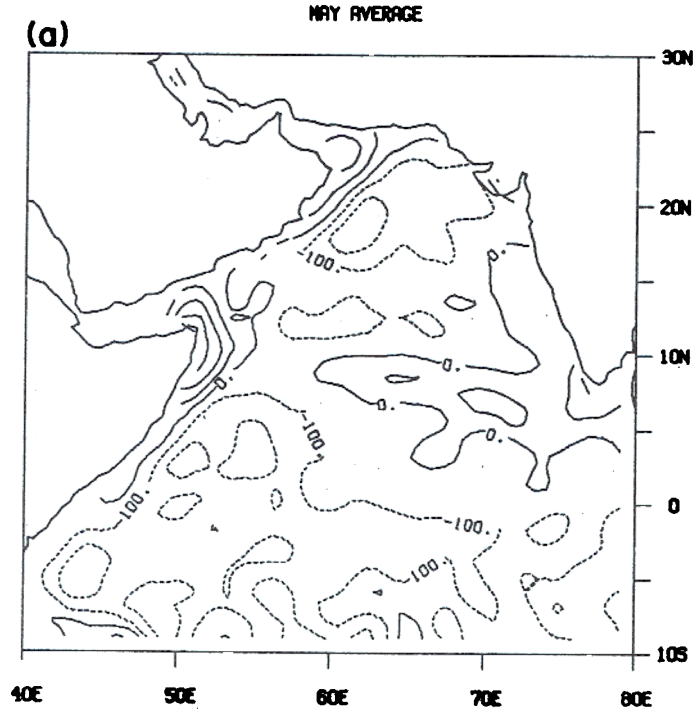
MAY AVERAGE
(a)
30N
20N
10N
0
10S
40E
50E
60E
70E
80E
-100.
0.
-100.
-100.
-100.
-100.
0.
0.
0.
0.

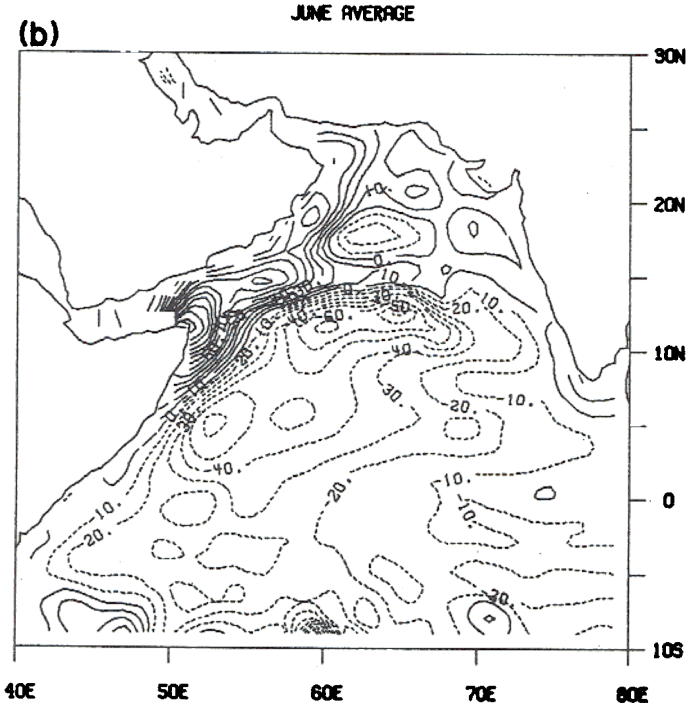
JUNE AVERAGE
(b)
30N
20N
10N
0
10S
40E
50E
60E
70E
80E
10.
0
10.
20.
10.
40.
30.
20.
10.
40.
10.
20.
20.
10.
10.
20.

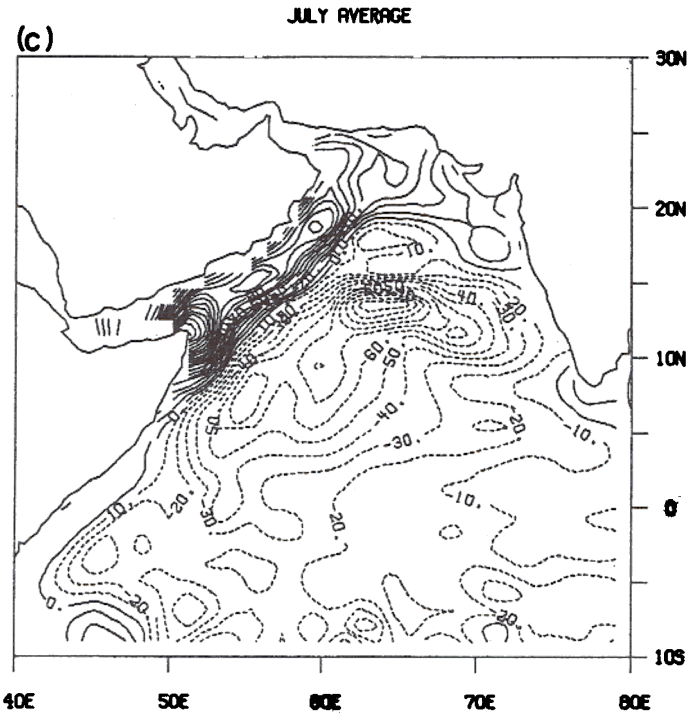

FIG. 20. Average wind stress curl. (a) May. Contour interval is 7×10^{-8} Nt m^{-3}. Labels are scaled by 10^9. (b) June. Contour interval is 2×10^{-7} Nt m^{-3}. Labels are scaled by 10^8. (c) July. Contour interval is 3×10^{-7} Nt m^{-3}. Labels are scaled by 10^8.

generally good agreement between their observations and the model results, especially during the onset phase of the southwest monsoon. For instance, their Fig. 5 and our Fig. 10 both show the doming of the isotherms (thinning of the upper layer) off the Somali Coast between 5°S and the equator with the surface current turning offshore at about 2°N during the early stages of the monsoon. In the later stages of the monsoon, the offshore flow in the model between the northern and southern gyres in the Somali Current is not as strong as in SWALLOW *et al.* (1983) observations. The model is also unable to reproduce the strong upwelling wedge between the two gyres, as there are no thermodynamic effects and no exchange of water between the upper and lower layers, although the wedge can be inferred from the vertical velocity, and of course it cannot reproduce the surface density fronts that they observed.

There are several possible explanations for the discrepancies between the model and the observations. The model contains only one baroclinic mode, and for some of the observed features of the seasonal cycle, higher modes may be important. The model forcing is a climatological average forcing, and it is suspected that the interannual variability in the wind field may be large. The forcing also does not contain any information at periods shorter than two months, due to the fact that we used monthly mean winds. Shorter period fluctuations in wind stress may be important for triggering some of the observed shifts in the seasonal cycle.

The boundary imposed at 73°E is another limiting factor in the model. Even though the island chains along 73°E do effectively close off much of the Arabian Sea, there are still many

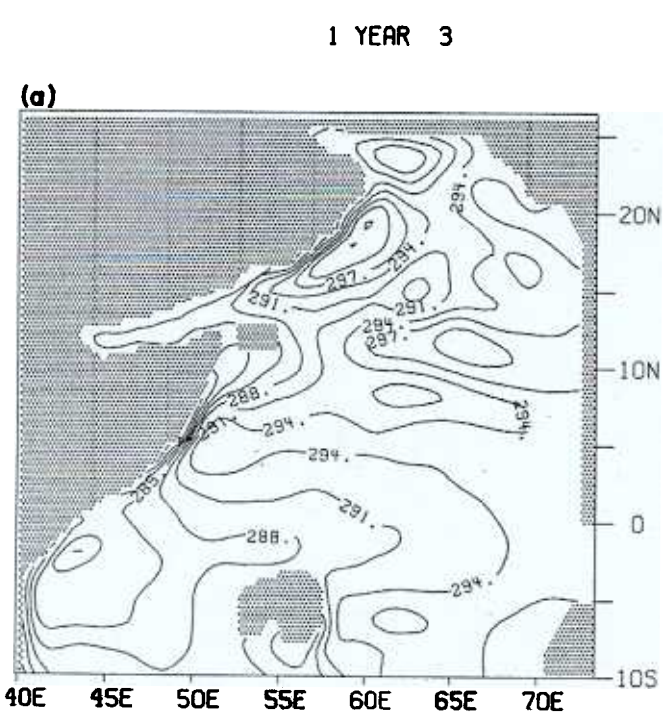
1 YEAR 3
(a)
294.
294.
297.
291.
291.
294.
297.
288.
294.
294.
294.
291.
288.
294.
20N
10N
0
10S
40E
45E
50E
55E
60E
65E
70E

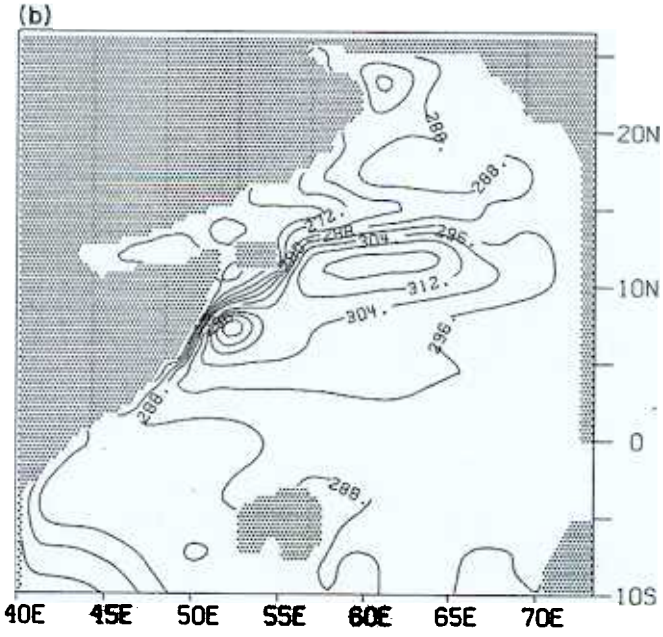
YEAR 3
(b)
288.
288.
272.
288
304.
296.
312.
304.
296.
288.
288.
20N
10N
0
10S
40E
45E
50E
55E
60E
65E
70E

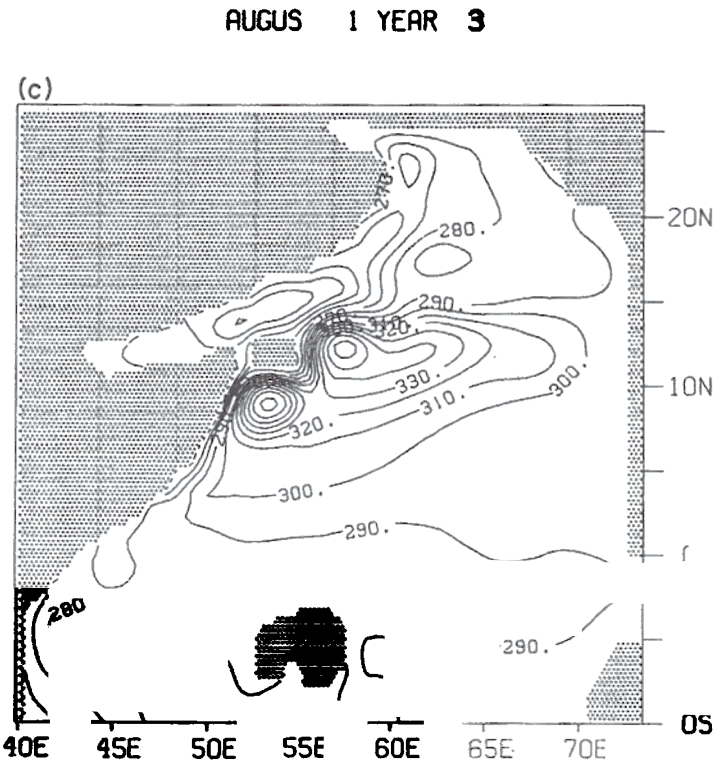

FIG. 21. Instantaneous upper layer thickness. (a) 1 June year 3. Contour interval is 3 m. (b) 1 July year 3. Contour interval is 8 m. (c) 1 August year 3. Contour interval is 10 m.

wide, deep channels through the islands. Observations indicate that at times there is considerable flow through these channels. The absence of the equatorial Indian Ocean east of 73°E also precludes the possibility of any remote forcing that has its origins in that region. Perhaps an even greater constraint on the model is the boundary at 10°S. ANDERSON and MOORE (1979) have indicated that the action of the southern hemisphere easterlies (the Trades) on the SEC and the EACC can have a large effect on the onset of the summer Somali Current. Since our model ends at 10°S, it cannot resolve the SEC, which is centered at 15°S, and therefore does not include the effects of the Trades. We hope to extend the model to include the entire Indian Ocean north of 25°S as soon as sufficient computing resources become available.

The only instability mechanism for generating the intense eddies in the model is that of barotropic or shear instability. It is possible that during some phases of the monsoon cycle, baroclinic instabilities become important. All told, however, this relatively simple model does a remarkable job of simulating the observed features of the seasonal cycle in the Somali Current.

5. SUMMARY AND CONCLUSIONS

We have shown that the seasonal circulation in the Arabian Sea can be modeled accurately if we have sufficient wind data. Using climatological mean winds, we have been able to reproduce

many of the observed features of the seasonal variation in the Somali Current system. We have every reason to believe that if we had better wind data, we could produce more accurate model simulations. Given accurate wind data on a timely basis, we could hindcast, and possibly forecast, the evolution of the surface currents in the Arabian Sea.

This model indicates that the entire seasonal cycle must be modeled in order to accurately simulate both the summer and winter monsoon onsets. The circulation patterns from the previous season greatly influence the development of the following season's circulation.

We have presented here only one particular case study from the model. In future papers we will look more closely at the dynamics of the circulation in the model. Work is underway to extend the model to include higher frequency wind data as input, and to investigate the effects of interannual variability in the wind field on the model currents.

Acknowledgements – We would like to dedicate this work to the leadership of John Swallow who convinced us all in his quiet way that the Indian Ocean was an interesting place to study.

This work was supported by the Office of Naval Research, Physical Oceanography Branch. The interpolation for the wind data was done by Mr. Alex Meng. Comparison between our wind stress and the Hellerman and Rosenstein data was done by Mr. Edgar Pavia-Lopez. Programming assistance was provided by Mr. James D. Merritt and Mr. Chen-Tan Lin. Typing services were expertly handled by Ms. Pat Teaf and Ms. Helen McKelder. We would also like to thank our colleagues for their many comments and suggestions.

REFERENCES

ADAMEC, D. and J. J. O'BRIEN (1978) The seasonal upwelling in the Gulf of Guinea due to remote forcing. *Journal of Physical Oceanography*, 8, 1050–1060.

ANDERSON, D. L. T. and D. W. MOORE (1979) Cross-equatorial jets with special relevance to very remote forcing of the Somali Current. *Deep-Sea Research*, 26, 1–22.

BROWN, O. B., J. G. BRUCE and R. H. EVANS (1980) Evolution of sea surface temperature in the Somali Basin during the southwest monsoon of 1979. *Science*, 209 ,595–597.

BRUCE, J. G. (1973) Large scale variations of the Somali Current during the southwest monsoon, 1970. *Deep-Sea Research*, 20, 837–846.

BRUCE, J. G. (1979) Eddies off the Somali coast during the southwest monsoon. *Journal of Geophysical Research*, 84, C12, 7742–7748.

BRUCE, J. G. (1983) The wind field in the western Indian Ocean and the related ocean circulation. *Monthly Weather Review*, 111, 1442–1452.

BUSALACCHI, A. J. and J. J. O'BRIEN (1980) The seasonal variability in a model of the tropical Pacific. *Journal of Physical Oceanography*, 10, 1929–1951.

CAGLE, B. J. and R. WHRITNER (1981) *Arabian Sea project of 1980 – Composites of infrared images.* Technical report, Office of Naval Research, Western Regional Office, Pasadena, CA, 61pp.

CAMERLENGO, A. L. and J. J. O'BRIEN (1980) Open boundary conditions in rotating fluids. *Journal of Computational Physics*, 35, 12–35.

CANE, M. A. (1979a) The response of an equatorial ocean to simple wind stress patterns: I. Model formulation and analytical results. *Journal of Marine Research*, 37, 233–252.

CANE, M. A. (1979b) The response of an equatorial ocean to simple wind stress patterns: II. Numerical results. *Journal of Marine Research*, 37, 253–299.

CHARNEY, J. G. (1955) The generation of ocean currents by the wind. *Journal of Marine Research*, 14, 477–498.

COX, M. D. (1970) A mathematical model of the Indian Ocean. *Deep-Sea Research*, 17, 47–75.

COX, M. D. (1976) Equatorially trapped waves and the generation of the Somali Current. *Deep-Sea Research*, 23, 1139–1152.

COX, M. D. (1979) A numerical study of Somali Current eddies. *Journal of Physical Oceanography*, 9, 311–326.

DÜING, W. (1978) The Somali Current: Past and recent observations. *Review Papers of Equatorial Oceanography: FINE Workshop Proceedings*, Nova/N.Y.I.T. University Press.

FINDLAY, A. G. (1866) *A directory for the navigation of the Indian Ocean.* Richard Holmes Laurie, London, 1062 pp.

HASTENRATH, S. and P. J. LAMB (1979) *Climatic atlas of the Indian Ocean*, University of Wisconsin Press.

HELLERMAN, S. and M. ROSENSTEIN (1983) Normal monthly wind stress over the world ocean with error estimates. *Journal of Physical Oceanography*, 13, 1093–1104.

HURLBURT, H. E. (1974) The influence of coastline geometry and bottom topography on the eastern ocean circulation. Ph.D. dissertation, Florida State University, 104pp.

HURLBURT, H. E. and J. D. THOMPSON (1976) A numerical model of the Somali Current. *Journal of Physical Oceanography*, 6, 646–664.

KINDLE, J. C. (1979) Equatorial Pacific Ocean variability – seasonal and El Niño time scales. Ph.D. dissertation, Florida State University, 134pp.

LIN, L. B. and H. E. HURLBURT (1981) Maximum simplification of nonlinear Somali Current dynamics. *Monsoon dynamics*, M. J. LIGHTHILL and R. P. PEARCE, editors, Cambridge University Press.

SCHOTT, F. (1983) Monsoon response of the Somali Current and associated upwelling. *Progress in Oceanography*, 12, 357–381.

SWALLOW, J. C. and M. FIEUX (1982) Historical evidence for two gyres in the Somali Current. *Journal of Marine Research*, 40, supplement, 747–755.

SWALLOW, J. C., R. L. MOLINARI, J. G. BRUCE, O. B. BROWN and R. H. EVANS (1983) Development of near-surface flow pattern and water mass distribution in the Somali Basin, in response to the southwest monsoon of 1979. *Journal of Physical Oceanography*, 13, 1398–1415.